Silicon (2024) 16:5431–5438
https://doi.org/10.1007/s12633-024-03093-7

RESEARCH

Effect of Different Ambient Atmospheres on the Damage Caused to Silicon by 1064-nm Laser Pulses

Ming Guo[1] · Yong-xiang Zhang[2] · Wen-ying Zhang[1] · Nan Li[1] · Ji-xing Cai[3]

Received: 9 December 2023 / Accepted: 11 July 2024 / Published online: 23 July 2024

Abstract

A nanosecond-pulsed laser with a wavelength of 1064 nm was used to irradiate silicon, and the concentration of water mist and smoke was characterized through light transmission. The drift and scattering effects of the laser propagation atmosphere (water mist and smog environment) on the laser and the influence of different ambient atmospheres on the effect of the laser irradiation on silicon were studied. Research has shown that when a laser passes through a water mist environment, as the laser transmission ratio increases, the diameter of the exit spot increases, and the diameter of the damage induced to single-crystal silicon increases approximately linearly. The erosion damage is enhanced, and a mixture of heat and stress damage occurs. Smoke is a simulated haze environment, and the attenuation effect of the aerosol content on the laser in a smoke environment depends on the particle size and concentration. When the laser transmission ratio is the same, the diameter of the particles is small, and the corresponding particulate matter concentration is large. The smaller the particle size, the larger the particle concentration corresponding to a different laser transmission ratio. When the laser energy of the target is the same, the shape and size of the export laser change as the laser passes through fog; furthermore, the damage shape is no longer circular, but it is rather stretched and deformed along a specific direction. This study can provide a reference for laser processing, far-field laser applications, and atmospheric optics.

Keywords Nanosecond laser · Silicon · Damage · Water mist · Smoke

1 Introduction

Silicon is a fundamental material for optoelectronic devices, and it is widely used in the military and production fields as well as daily life. Lasers are often used as excellent light sources due to their good directionality and other characteristics. The damage caused by lasers to silicon can lead to the degradation or failure of the optoelectronic system; thus, studying the laser damage to silicon is of great significance. A lot of research has been performed on the damage caused by lasers to silicon in air [1–4], but different purposes require very different atmospheres for the laser transmission path. The ambient atmosphere is an important factor affecting laser transmission [5–7] as it can have a significant impact on the damage induced by lasers to silicon. Momeni [8] experimentally investigated the removal rate of silicon wafers in distilled water and analyzed the mechanism of nanosecond-laser ablation in single-pulse and double-pulse processes. It was found that double-pulse laser ablation resulted in a greater ablation amount and a larger average nanoparticle size. Yang [9] studied the microstructure formed on the surface of monocrystalline silicon under three gas environments using 532-nm nanosecond-pulsed laser irradiation. The study found that the background gas played an important role in determining the silicon surface morphology and the ablation efficiency. The ripple microstructure at the edge of the irradiation area was believed to be caused by the cooling of the surface tension waves. Yuan [10] used femtosecond-laser pulses to irradiate monocrystalline silicon in SF_6, air, and vacuum environments to study the evolution of the silicon surface microstructure.

✉ Yong-xiang Zhang
laserqit@sina.com

[1] Institute for Interdisciplinary Quantum Information Technology, Jilin Engineering Laboratory for Quantum Information Technology, Jilin Engineering Normal University, Changchun 130052, China

[2] Changchun Institute of Electronic Science and Technology, Changchun 130000, China

[3] Changchun University of Science and Technology, Changchun 130000, China

By comparing the microstructures obtained under the different atmospheres, it was found that the number density of the peaks varied. The peak height obtained in SF_6 was the highest, while the peak height obtained in air was the lowest. The formation of microstructures is mainly determined by laser ablation, chemical etching, and oxidation.

In this work, a nanosecond laser with a wavelength of 1064 nm was used to irradiate silicon after transmission in water mist and smoke environments. The effects of the water mist and smoke environments on the laser drift, absorption, and other factors affecting laser transmission were studied, and possible damage mechanisms for the different laser transmission paths were explored. This study can provide a reference for laser processing and the use of laser weapons.

2 Theory of the Thermal and Mechanical Damage Caused to Silicon by Lasers

Silicon is an excellent semiconductor, and thermal damage can occur after it is irradiated by a pulsed laser. Thermal damage includes melting and ablation splashing, while mechanical damage mainly includes cleavage and the formation of cracks. The process of laser interaction with silicon involves the interaction between the particles in silicon, such as electrons and lattice phonons, and the laser electromagnetic field with a consequent absorption of energy from silicon. Various particles that are in a nonequilibrium state relax toward the equilibrium state and convert the absorbed laser energy into disordered thermal energy. The thermal energy diffuses in silicon through thermal conduction. When the temperature exceeds the melting and boiling points of silicon, the material melts and vaporizes.

Silicon crystals are anisotropic, and the thermal conductivity also exhibits anisotropy. The thermal conductivity coefficient is a second-order tensor (k), and the heat flux density vector can be expressed as:

$$q = -k \cdot \nabla T = -k_{ij}\frac{\partial T}{\partial x_j}e_i \tag{1}$$

We now consider a small-volume element of the silicon material; the heat flowing through its surface plus the heat generated inside it is equal to the energy accumulated in the small-volume element; then, the heat conduction equation inside silicon is:

$$-\nabla \cdot q + g = \rho c\frac{\partial T}{\partial t} \tag{2}$$

where q is the heat flux density vector, g is the volumetric heat source, ρ is the silicon density, and c is the specific heat capacity.

If the heat flux density vector expression is introduced, and the thermal conductivity coefficient does not does not vary spatially, the thermal conductivity equation for the silicon material is:

$$k_{ij}\frac{\partial^2 T}{\partial x_i \partial x_j}e_i + g = \rho c\frac{\partial T}{\partial t} \tag{3}$$

According to the linear thermal stress theory, temperature changes can cause strain, and stress can also cause strain. Therefore, the total strain of a microelement is obtained by adding the strain caused by both temperature and stress. Hooke's law can be extended to include thermal stress and strain as follows:

$$\left.\begin{aligned}\varepsilon_x &= \frac{\partial u_x}{\partial x} = \frac{1}{E}[\sigma_x - \mu(\sigma_y + \sigma_z)] + \beta T\\ \varepsilon_y &= \frac{\partial u_y}{\partial y} = \frac{1}{E}[\sigma_y - \mu(\sigma_z + \sigma_x)] + \beta T\\ \varepsilon_x &= \frac{\partial u_z}{\partial z} = \frac{1}{E}[\sigma_x - \mu(\sigma_y + \sigma_z)] + \beta T\end{aligned}\right\} \tag{4}$$

$$\gamma_{xy} = \frac{\tau_{xy}}{G}, \gamma_{yz} = \frac{\tau_{yz}}{G}, \gamma_{zx} = \frac{\tau_{zx}}{G} \tag{5}$$

where β is the linear expansion coefficient of monocrystalline silicon, and E is Young's modulus. The shear elastic modulus (G) and bulk stress (Θ) are expressed as:

$$G = \frac{E}{2(1+\mu)}, \Theta = \sigma_x + \sigma_y + \sigma_z \tag{6}$$

where μ is Poisson's ratio.

The strain vector is represented as:

$$\begin{pmatrix}\varepsilon_x\\ \varepsilon_y\\ \varepsilon_z\\ \gamma_{xy}\\ \gamma_{yz}\\ \gamma_{zx}\end{pmatrix} = \begin{pmatrix}\frac{\partial u_x}{\partial x}\\ \frac{\partial u_y}{\partial y}\\ \frac{\partial u_z}{\partial z}\\ \frac{\partial u_y}{\partial x} + \frac{\partial u_x}{\partial y}\\ \frac{\partial u_z}{\partial y} + \frac{\partial u_y}{\partial z}\\ \frac{\partial u_x}{\partial z} + \frac{\partial u_z}{\partial x}\end{pmatrix} \tag{7}$$

where u_x, u_y, and u_z are the displacements in the x-, y-, and z-directions.

According to Hooke's law, the stress vector can be obtained as:

$$\sigma = C(\varepsilon - \varepsilon_0) \tag{8}$$

$$\sigma = (\sigma_x\ \sigma_y\ \sigma_z\ \tau_{xy}\ \tau_{yz}\ \tau_{zx})^T \tag{9}$$

Silicon crystal has the atomic structure of diamond, and the symmetry stiffness matrix of the crystal system can be expressed as:

$$C = \begin{pmatrix} C_{11} & C_{12} & C_{12} & & & \\ C_{12} & C_{11} & C_{12} & & & \\ C_{12} & C_{12} & C_{11} & & & \\ & & & C_{44} & & \\ & & & & C_{44} & \\ & & & & & C_{44} \end{pmatrix} \tag{10}$$

3 Experimental setup

The experimental system to induce damage to silicon using a nanosecond-pulsed laser is shown in Fig. 1. The laser was purchased from Changchun New Industry Optoelectronics Company; the laser model is LPS-1064-L, and the wavelength is 1064 nm. The laser transmission length of the environmental chamber is 700 mm, and it has a built-in combustion tray, which is connected to a controllable water mist generator and a temperature and humidity measurement meter. Rotatable blades are installed in the environmental chamber to homogenize water mist and smoke. The water mist generator is an ultrasonic humidifier that adjusts the amount of mist produced based on the power of the ultrasonic waves. Smoke is generated by the combustion of the smoke cake, and the concentration of smoke is adjusted by controlling the quality of the smoke cake.

After passing through the environmental cavity, the nanosecond laser beam is divided by a spectroscope, and 50% of the energy enters the J-50 MB-YAG energy meter to measure the pulse energy. The other part of the beam is vertically incident on the surface of the silicon sample after passing through a focusing lens with focal length $f' = 200$ mm. The silicon target is clamped on a two-dimensional translation platform. In the experiment, the crystal plane orientation of the silicon target is (100), and the silicon wafer has a length, width, and thickness of 20, 20, and 0.5 mm, respectively.

4 Results and Analysis

In the experiment, the concentration of water mist and smoke was measured using the light transmission method, and the extinction performance of the fog environment was characterized in terms of the laser transmittance, which is the ratio of the laser energy after the laser passes through the chamber to the laser energy before it enters the chamber. The table of extinction coefficients for foggy environments is shown in Table 1 and Table 2.

The diameter of the laser at the entrance of the environmental cavity is 1.0 mm. When the laser passes through environments with different concentrations of water mist, the size of the light spot at the exit changes; in particular, this spot size changes with the laser transmission ratio through water mist, as shown in Fig. 2. From Fig. 2, it can be seen that under the action of the laser with three different energies, the spot size increases with the increase in laser transmission ratio. The absorption of the 1064-nm-wavelength light by the water molecules in water mist is very small, and the attenuation mainly originates from scattering. When the laser transmission ratio is less than 20%, the water mist is dense, and most of the laser energy is scattered by the water mist molecules and dissipated through molecular motion in the environmental chamber. The energy of the laser that penetrates becomes weaker Due to the Gaussian distribution of the laser beam, the intensity is the highest at the center of the laser beam, and the center beam penetrates the water

Table 1 Extinction coefficients under water mist conditions

Transmission atmosphere	Extinction coefficient	Humidity
Water mist	0.12	79.3%
Water mist	0.59	87.2%
Water mist	0.74	89.8%
Water mist	0.85	93.7%

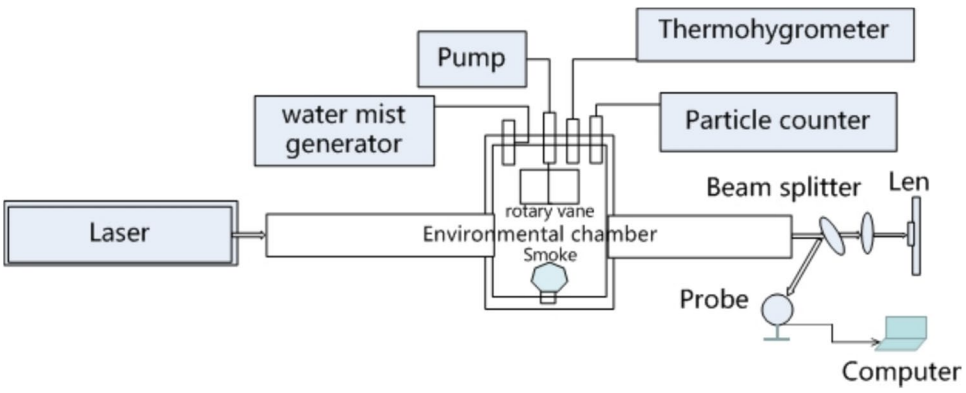

Fig. 1 Experimental system for irradiating silicon with the nanosecond-pulsed laser

Table 2 Extinction coefficients under smoke conditions

Transmission atmosphere	Extinction coefficient	PM 0.3	PM 0.5	PM 1.0	PM 2.5	PM 5.0	PM 10
smoke	0	33446.0	9500.0	1762.0	76.0	0	0
smoke	0.4	422457.0	140329.0	127125.0	73093.0	33050.0	16461.0
smoke	0.423	428425.0	142392.9	129746.0	75665.9	34094.9	17491.6
smoke	0.58	547686.3	156357.7	164331.2	96027.2	43468.3	22425.0
smoke	0.86	653295.5	226915.7	206841.8	125865.3	60521.3	32377.7

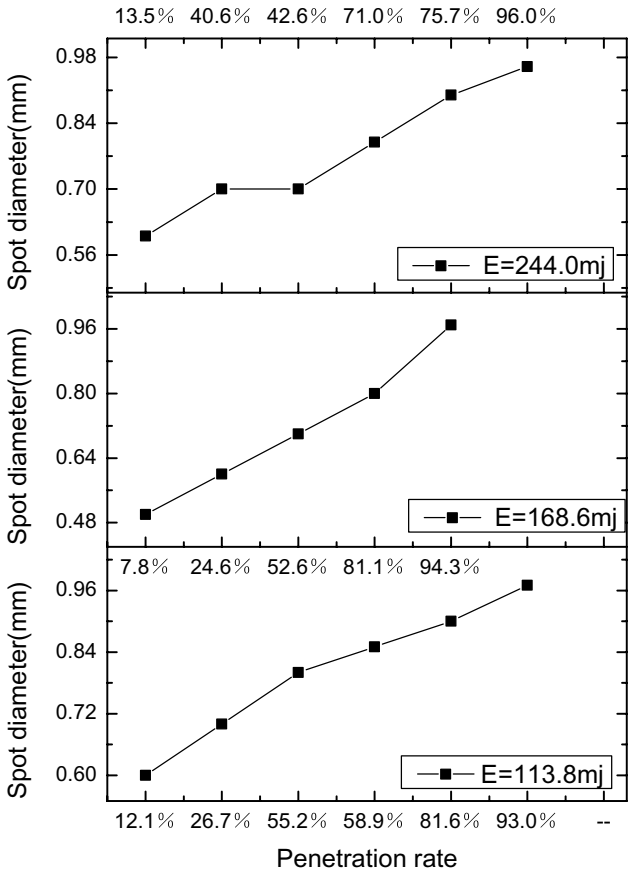

Fig. 2 Variation in the Spot Size with Laser Transmission Ratio through Water Mist

mist to form a spot. As the transmission ratio decreases, the size of the laser spot decreases.

By comparing the three incident laser energies, it can be seen that when the laser energy is 113.8 mJ, the diameter of the penetrating laser spot is relatively large. When the diameter of the exit spot is about 0.97 mm, the corresponding laser transmission ratio ranges from 93.0% to 96.0%. The increase in laser energy can exacerbate the ionization of gas molecules and water mist molecules near the laser beam, resulting in a greater loss of laser energy.

The laser transmission ratio through water mist is an important parameter that affects the laser damage caused to silicon. The laser damage morphology of monocrystalline silicon for different laser transmission ratios of water mist atmosphere conditions is shown in Fig. 3. From Fig. 3, it can be seen that different laser transmission ratios result in significant differences in the damage morphology. As the laser transmission ratio increases, the ablation area of monocrystalline silicon increases, and molten pits appear. When the laser transmission ratio exceeds 41.7%, crack damage occurs at the edge of the damage spot, and the depth at which the laser energy is absorbed in monocrystalline silicon increases. The internal temperature of silicon increases, and thermal expansion occurs. When subjected to surrounding constraints, thermal stress is generated, resulting in a combined damage due to both heat and stress. When the laser transmission ratio is lower than 20%, the water mist is dense, and the corresponding damage morphology is shown in Fig. 3(a)–(c). The circular laser spot undergoes distortion and becomes elliptical in shape. When the laser transmission ratio is 87.2%, the damage shape is approximately circular. In the process of laser transmission, in addition to the scattering and refraction of light from the water mist molecules, the environmental cavity through which the laser beam propagates is equipped with a uniform water mist rotating plate, and turbulent vortices are generated in the laser transmission path. When the laser passes through this cavity, the intensity and phase of the light waves exhibit random fluctuations in time and space, resulting in intensity flicker, drift, and other distortion phenomena of the light spot.

The variation in the damage diameter of monocrystalline silicon with the water mist transmittance is shown in Fig. 4. From Fig. 4, it can be seen that as the laser transmission ratio increases, the damage diameter of monocrystalline silicon increases approximately linearly. The damage diameter of monocrystalline silicon is closely related to the size of the laser spot that illuminates monocrystalline silicon, and the laser spot increases with the increase in laser transmission ratio,

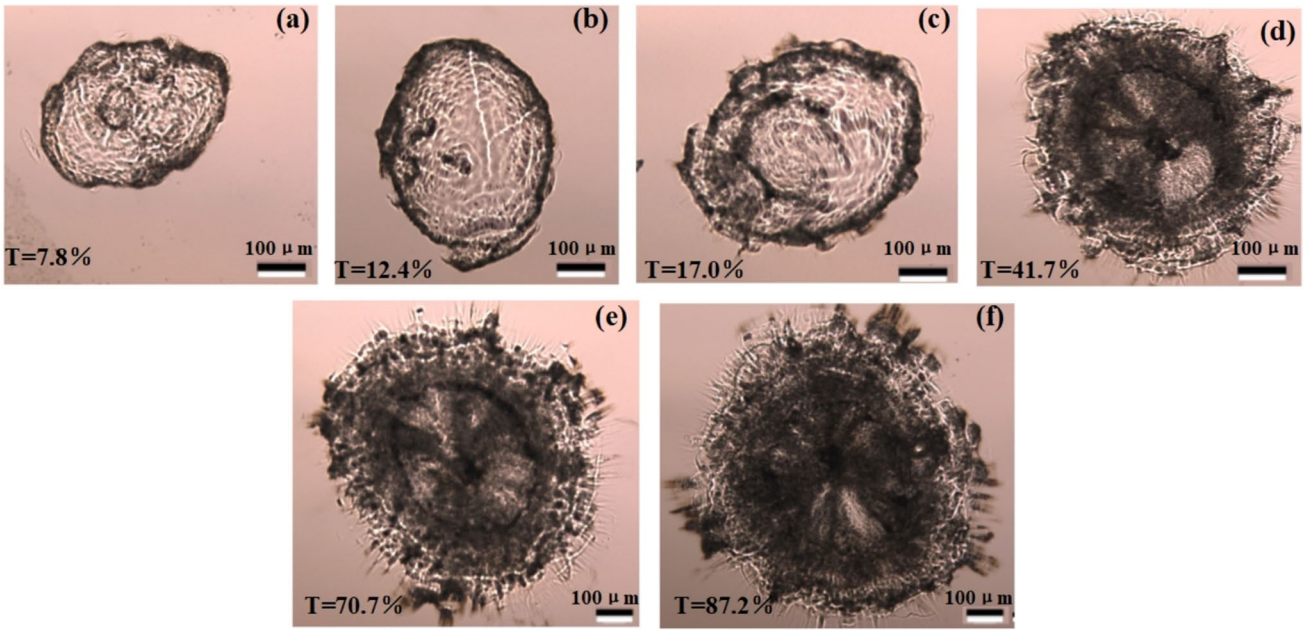

Fig. 3 Damage morphology under water mist conditions ((**a**) T=7.8%, (**b**) T=12.4%, (**c**) T=17.0%, (**d**) T=41.7%, (**e**)T=70.7%, (**f**) T=87.2%)

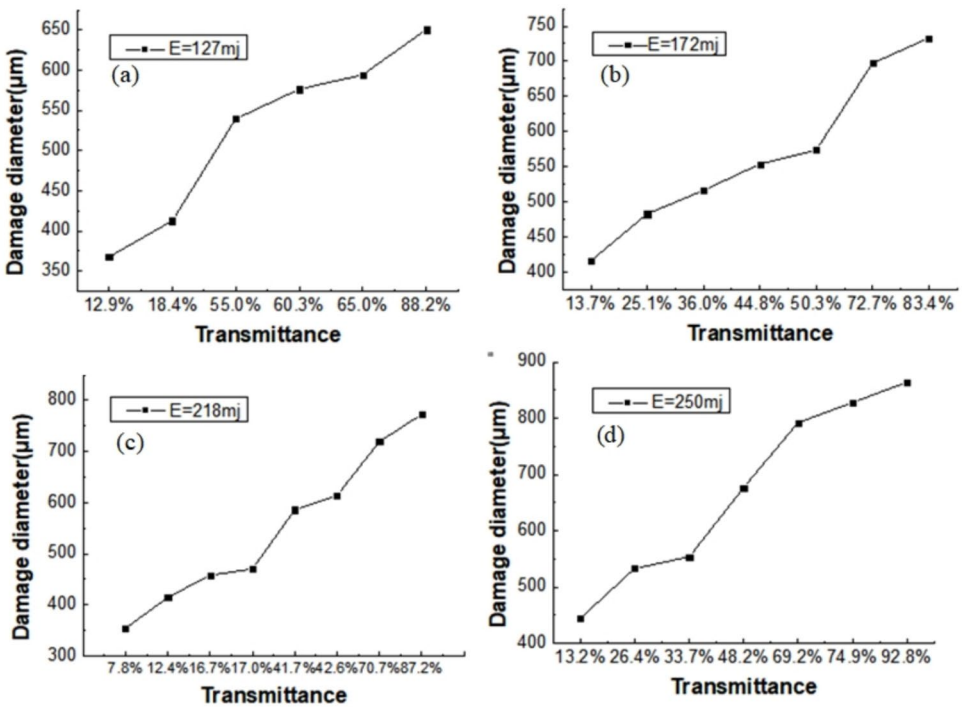

Fig. 4 Change in the Damage Diameter with the Water Mist Transmittance ((**a**) E=127mj, (**b**) E=172mj, (**c**) E=218mj, (**d**) E=250mj)

so the damage diameter of monocrystalline silicon also increases. In the figure, four different incident laser energies are considered; in all cases, the laser energy is much greater than the laser energy required for silicon ablation. With the increase in laser energy, the vaporization point is eventually reached, and at vaporization temperatures, the thermal conductivity coefficient decreases, the surface ablation area increases, and the damage diameter increases. By comparing Fig. 4(c) and Fig. 4(d), it is observed that when the laser transmission ratio is about

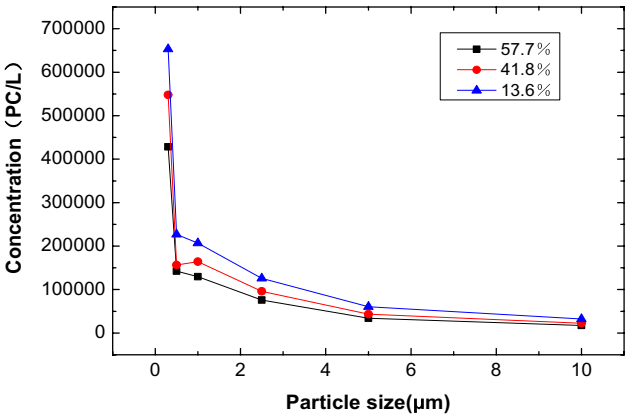

Fig. 5 Relationship between the particle size and particle number concentration under fixed laser transmittance conditions

70%, the damage diameter is as large as 72.7 μm, which corresponds to an increase of 10%.

The complexity of the smoke environment, including particle concentration, composition, and particle size, is an important factor affecting the laser transmission characteristics, and its parameters determine the laser energy transmittance. The relationship between the particle size and particle concentration for a fixed laser transmittance is shown in Fig. 5. The main components of the smoke cake used in this experiment are sulfur, cellulose, lignin, etc. After combustion, sulfur dioxide and inhalable particulate matter are produced, which represents a similar composition to that of haze. From Fig. 5, it can be seen that (1) the attenuation coefficient of the aerosol on the laser depends on the particle size. When the laser transmission ratio is the same, the particle diameter is 0.3 μm, and the corresponding particle concentration is maximum. The diameter of particulate matter varies from 0.3 to 10 μm, while the concentration of particulate matter varies from 6.53×10^5 to 3.23×10^4 PC/L, which represents a 95% decrease in concentration. For particle sizes greater than 1.0 μm, light attenuation involves scattering, reflection, and absorption. Smoke particles are always in motion, and the positive and negative charges of particles have the characteristic of non coincidence. They can be regarded as electric dipoles, and under the action of electromagnetic radiation, they can change the transmission characteristics of the original laser and produce attenuation in the direction of laser transmission. (2) When particle size is the same, as the particle concentration increases, the laser transmission ratio decreases, and the particle size decreases. When the particle size is less than 0.5 μm, the difference in particle concentration corresponding to different penetration rates is greater. When the particle size is 10 μ m, the concentration of aerosol particles at each transmission ratio is basically the same.

The damage morphology of single-crystal silicon caused by nanosecond laser transmission in a smoke environment is shown in Fig. 6. The water, carbon dioxide, oxygen, and other substances in the air do not absorb 1.06-micron laser radiation, which belongs to the so-called "atmospheric window". Theoretical and experimental research demonstrated that for 1064-μm lasers, the main factors affecting laser transmission are aerosol absorption and scattering, which convert the laser radiation energy into thermal energy during the absorption and scattering processes. The laser transmission ratio is 12.3%, and silicon is damaged by laser ablation in a small area. The damage appears in a porous form with clear edges. When the laser transmission ratio is 60.6%, the damage area is about twice that observed for a transmission ratio of 12.3%. The center of the laser irradiation spot has a molten pit, with molten material being accumulated and protruding at the center edge, and stress damage occurring at the edge.

The damage morphology of monocrystalline silicon in air, water mist, and smoke transmission environments was compared and analyzed for fixed laser energies, as shown in Fig. 7.

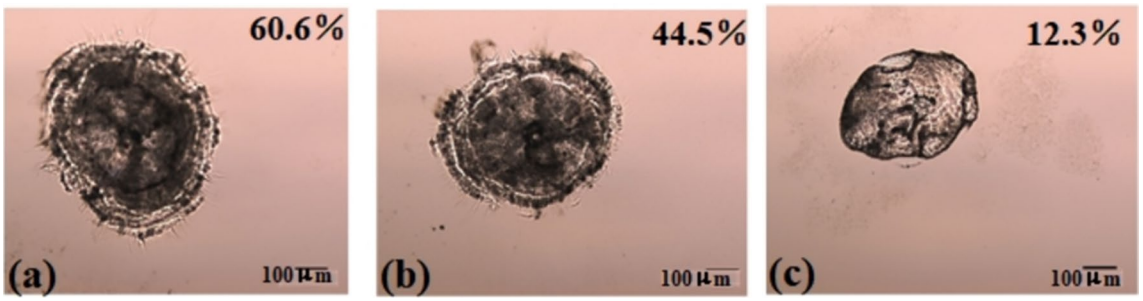

Fig. 6 Damage morphology under smoke transmission conditions ((**a**) T=60.6%, (**b**) T=44.5%, (**c**) T=12.3%)

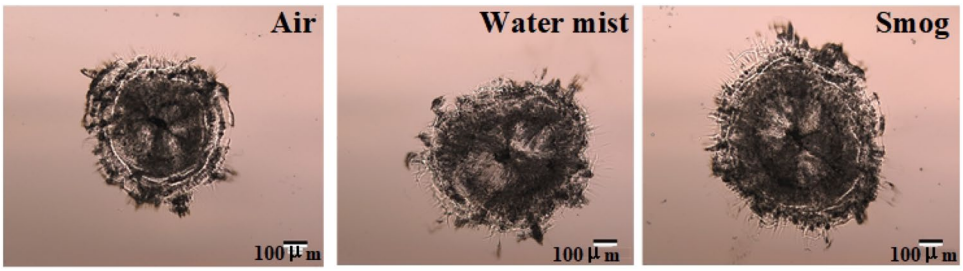

Fig. 7 Comparison of the damage morphology under air and fog conditions

The laser energy on the target was 55 mJ in all cases. Figure 7(b) shows the water mist transmission environment with a laser transmission ratio of 12.8%, and Fig. 7(c) shows the smoke transmission environment with a laser transmission ratio of 40.0%. Although the laser energy reaching the target is the same in all cases, in fog transmission, the shape and size of the exit laser spot change, and the damage morphology is no longer circular, but it is rather deformed through stretching in a specific direction. The average diameters of the damage in air, water mist, and smoke transmission are 596.1, 650.4, and 662.9 μm, respectively. Under the transmission conditions of water mist and smoke, the energy distribution on the cross section of the laser beam fluctuates and the beam expands, resulting in an increase in the target spot size and a larger damage diameter.

5 Conclusion

In this study, a near-infrared nanosecond-pulsed laser was utilized to irradiate silicon. The impact of the laser propagation atmosphere on the damage caused to silicon was analyzed based on the physical mechanisms of absorption and scattering during laser propagation in the atmosphere. The transmission ratio of the laser was used to characterize the concentration of water mist and smoke. The absorption of 1064-nm-wavelength light by the water molecules in water mist is very small, and the attenuation mainly originates from scattering. When the laser transmission ratio is less than 20%, the water mist is dense, and most of the laser energy is scattered by the water mist molecules and dissipated through the molecular motion of the environmental chamber; furthermore, The penetrating laser energy has weakened as the transmission ratio decreases, the size of the laser spot decreases. As the laser transmission ratio increases, the damage diameter of monocrystalline silicon increases approximately linearly. Under smoke environment conditions, for a given particle size, the laser transmission ratio decreases as the particle concentration increases. For a given laser energy reaching the target, when the laser is transmitted through fog, due to random fluctuations in the light intensity and phase in time and space, the exit spot expands, and the damage diameter increases.

Author contributions All authors contributed to the study conception and design. The experimental operations were mainly completed by [Nan Li] and [Jixing Cai], data collection and analysis were performed by [Yongxiang Zhang] and [Wen-ying Zhang]. The first draft of the manuscript was written by [Ming Guo], all authors commented on previous versions of the manuscript. All authors read and approved the final manuscript.

Funding This research was supported by "Science and Technology Plan of Jilin Province"(Grant No. 20230101241JC),"Horizontal projects (Grant numbers[2022hx67KJ] and [2022hx68KJ])", Ming Guo has received research support from Jilin Xintuowei Teaching Instrument and Equipment Co", Ltd. and Jilin Taihefeng Technology Development Co., Ltd", "Science and Technology Development Plan Project of Jilin Province in 2022, Quantum information Technology Innovation Team" (Grant number [20220508136RC]).

Data Availability Data are contained within the article.

Declarations

Ethics Approval Not applicable.

Consent to Participate All institutions and authors agree to participate in this manuscript, and doesn' t contain any material from third parties.

Consent for Publication All authors have read and agreed to the published version of the manuscript.

Competing Interests The authors declare no competing interests.

References

1. Chen L, Liu Z, Guo C (2022) Nanosecond laser-induced controllable periodical surface structures on silicon. Chin Opt Lett 20:013802
2. Choi S, Jhang KY (2014) Thermal damages on the surface of a silicon wafer induced by a near-infrared laser. Opt Eng 53:017103
3. Ohmura E, Fukuyo F, Fukumitsu K (2006) Internal modified-layer formation mechanism into silicon with nanosecond laser. J Achiev Mater Manuf Eng 17:381–384
4. Zeng X, Mao XL, Greif R (2005) Experimental investigation of ablation efficiency and plasma expansion during femtosecond and nanosecond laser ablation of silicon. Appl Phys 80:237–241
5. Juntong Z, Su Z, Qiang F (2020) Laser polarization characteristics of visible light band in different humidity environments. Infrared Laser Eng 49:20200057-1–20200057-7

6. Ricklin JC, Hammel SM, Eaton FD (2006) Atmospheric channel effects on free-space laser communication. J Opt Fiber Commun Rep 3(2):111–158
7. Al Naboulsi MC, Sizun H, de Fornel F (2004) Fog attenuation prediction for optical and infrared waves. Opt Eng 43:319–329
8. Momeni A, Mahdieh MH (2015) Double-pulse nanosecond laser ablation of silicon in water. Laser Phys Lett 12:076102
9. Hongdao Y, Xiaohong Li, Guoqiang Li (2011) Surface morphology of silicon induced by 532 nm nanosecond laser under different ambient atmospheres. Chin J Opt 4:7
10. Chunhua Y, Xiaohong Li, Duochang T (2010) Silicon surface microstructures induced by femtosecond laser pulses in different background gases. High Power Laser Part BeamS 22:2749–2753